Viscosity of graphene in lubricating oil, ethylene glycol and glycerol

Jianhong Bao[1,2] · Rodolphe Heyd[2,3] · Gilles Régnier[1] · Amine Ammar[2] · Jorge Peixinho[1]

Abstract

This paper reports the results of an experimental investigation of graphene particle suspensions in lubricating oil, ethylene glycol and glycerol-based fluids. Graphene particles of different specific surface area show variation in the viscosity depending on the shear rate and the temperature. The lubricating effect, e.g., reduction in the viscosity compared to the base fluid, is observed for the concentration (below 0.4 mass%) in lubricating oil and glycerol. In the range of parameters studied (e.g., concentration below 1 mass% and temperature up to 80 °C), the activation energy slightly decreases. The enhancement of viscosity with graphene volume fraction is larger for ethylene glycol.

Graphical abstract

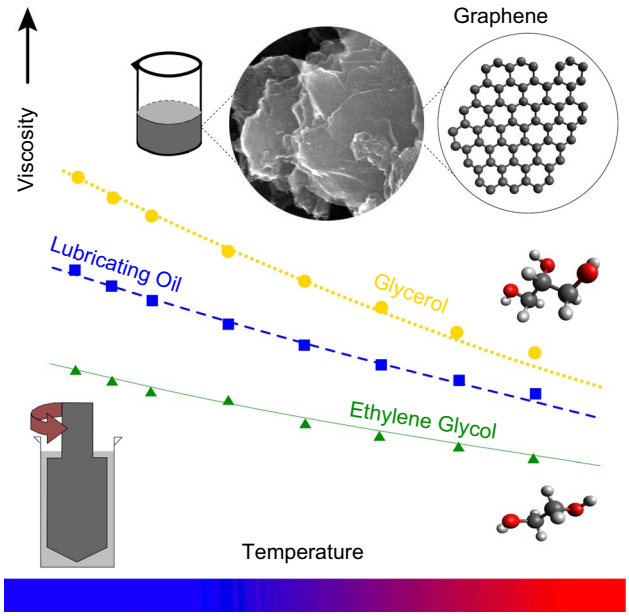

Keywords Graphene · Viscosity · Lubricating oil · Ethylene glycol · Glycerol

✉ Jorge Peixinho
jorge.peixinho@cnrs.fr

[1] Laboratoire PIMM, Arts et Métiers Institute of Technologie, CNRS, Cnam, HESAM Université, 151 Boulevard de l'Hôpital, 75013 Paris, France

[2] LAMPA, Arts et Métiers Institute of Technologie, 2 Boulevard du Roceray, 40035 Angers, France

[3] LIRBEM, Cadi Ayyad University, ENS, Route d'Essaouira, 40000 Marrakech, Morocco

Introduction

The threat of global warming and the increasing frequency of environmental disasters shows the current urgency to improve energy efficiency. Heat transfer plays an important role in many industrial and technical applications ranging from cooling of heat engines or high-power transformers

to heat exchangers, refrigeration systems or power plants. Unfortunately, usual heat transfer fluids, such as water and polymer solutions, have relatively low thermal conductivity. One way to improve heat extraction is to combine the flow properties of heat transfer fluids with the high thermal conductivity of some solid materials, such as metals, metal oxides, or different carbon-based materials: carbon black [6], carbon nano-tubes [9], carbon nano-horns [4] or graphene nanoplatelets [29]. However, the use of suspensions with micrometer-sized solid materials can lead to complications, such as abrasion, sedimentation and clogging.

Graphene, a single-atom-thick sheet of hexagonally arrayed bonded carbon atoms, was elegantly obtained and characterized by Novoselov et al. [18] and is now one of the most studied materials. The importance of graphene nanoplatelets and their benefits have been investigated, and the following advantages have been mentioned [22]: (1) it is relatively easy to synthesize, (2) it has long suspension time (leading to stable particle suspensions), (3) graphene nanoplatelets have large surface area/volume ratio, and (4) present low erosion, corrosion and clogging. The dynamic viscosity of such suspensions is also an essential property for practical applications in heat transfer. Most of the scientific literature, which is about suspensions in water with sometimes surfactants/dispersants [1, 2, 10, 12, 19], evidenced that the graphene nanoplatelets concentration leads to a nonlinear increase in viscosity. In addition, several authors studied the viscosity of graphene nanoplatelets nanofluids [27] and showed a strong decrease with temperature. Mehrali et al. [16] prepared homogeneous graphene nanoplatelets suspensions using a high-power ultrasonic probe for the dispersion with concentrations 0.025, 0.05, 0.075 and 0.1 mass%, for three different specific surface areas of 300, 500 and 750 $m^2\ g^{-1}$. They measured the viscosity of aqueous graphene nanoplatelets versus shear rate at temperatures from 20 to 60 °C. It was observed that the viscosity decreased with the temperature but was sensitive to the concentration and the specific surface area. In water, the samples of graphene nanoplatelets suspension also exhibit shear-thinning, which can be explained as follows. At low shear rates, as the nanoplatelets rotate in the fluid, they gradually align themselves in the direction of increasing shear, producing then less resistance and hence a reduction in viscosity. When the shear rate is high enough, the maximum amount of possible shear ordering is attained and the aggregates break down to smaller sizes, decreasing viscosity [7, 25]. Iranmanesh et al. [11] also studied the viscosity and thermal conductivity of graphene nanoplatelets dispersed in distilled water and investigated the three influential parameters including concentration, temperature and specific surface area. They proposed correlations for the relative viscosity as a function of the different specific surface area, the concentrations and the temperatures.

For heat transfer applications, it is essential to properly assess the thermofluid behavior of graphene nanoplatelets for the adjustment of pumping power. The thermal conductivity, which is the ability of a material to transport energy in the form of heat, can be measured with different methods [5, 15]. The thermal conductivity of nanoplatelets suspensions depends on several factors [16], such as concentration, aspect ratio [23] and shape, material purity level and temperature [2]. Lee and Rhee [14] studied the thermal conductivity of ethylene glycol-based graphene nanoplatelets nanofluids, and they concluded that the thermal conductivity increased with concentration and temperature. Moreover, the thermal conductivity at high temperatures (above 40 °C) is enhanced by 3 and 5 h ultrasonic treatment. This can be explained by the faster heat transfer along the connected structures of the graphene nanoplatelets, which are easily formed at higher concentration and higher temperature [3, 15].

Another essential thermofluid property to consider for the adjustment of pumping power is the viscosity. Specifically, reliable quantitative dynamic viscosity data as a function of temperature, nanoplatelets concentration and shear rate are needed. Besides, there is a need for rheological properties of graphene nanoplatelets suspended in multiple base fluids [3], such as lubricating oil (LO), ethylene glycol (EG) and Glycerol (GL).

Materials and methods

Materials

Ethylene glycol (EG) (Lab-Honeywell), lubricating oil (LO) (Fuchs, ISO VG 68 RENEP CGLP) and Glycerol (GL) (Lab-Honeywell) were used as received. Their densities, melting point and boiling point temperature are indicated in Table 1. The graphene nanoplatelets (GNP) were purchased from the Nanografi Nanotechnology company (NNc) and used for the experiments. The dry powder of GNP has a black color, a purity of 99.9%, a particle diameter of 1.5 µm, thickness of 3 nm and a density of 1.9–2.2 g cm^{-3} at 20 °C (from NNc). Three kinds of GNP were used with different specific surface areas: 320, 530 and 800 $m^2\ g^{-1}$, labeled GNP3, GNP5 and GNP8. Figure 1 shows the scanning electron microscopy (SEM) images of GNP with different specific surface areas.

Table 1 Physical properties of tested fluids (data from the www.lab.honeywell.com and www.fuchs.com)

Fluids	Density/g cm^{-3}	Boiling/°C
LO	0.88	> 300
EG	1.11	195–197
GL	1.26	290

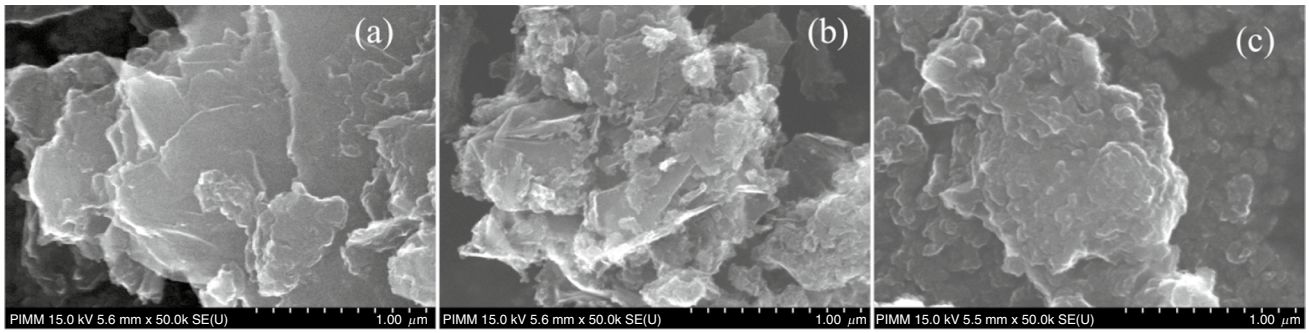

Fig. 1 SEM images of GNP made at a working distance of 5.6 or 5.5 mm and an electron high tension of 15 kV. **a** GNP3, **b** GNP5 and **c** GNP8

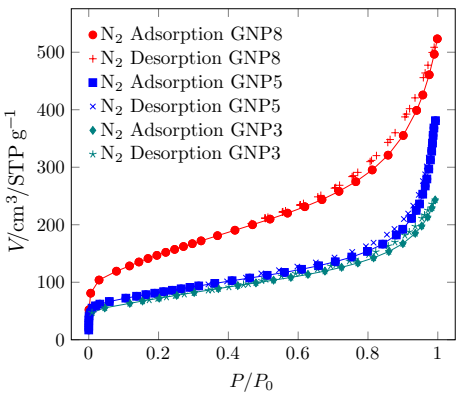

Fig. 2 Nitrogen adsorption–desorption isotherms for each GNP sample performed at 77 K (− 196.15 °C)

The images were performed with a scanning electron microscope Hitachi S-4800 at 15.0 kV of accelerating voltage. The sheet-like structure of the GNP has been well captured, with a lateral size at the micrometer length scale and an average thickness of 3 nm (in agreement with NNc). It can be seen clearly that the nanoplatelets are aggregated and overlap randomly.

Specific surface areas

The adsorption of nitrogen molecules N_2 (the adsorbate) to the surface of GNP (the adsorbent) creates a film, and the amount of adsorbate on the adsorbent as a function of its pressure at constant temperature is usually described as an isotherm. The isotherms, shown in Fig. 2, were carried out at 77 K (− 196.15 °C) using a gas adsorption instrument (Belsorp-max from BEL Japan, Inc.) after out-gassing the sample for several hours. The samples GNP3, GNP5, GNP8 masses were 73, 118 and 31 mg, respectively. A slight hysteresis is observed at high pressures. The adsorption isotherms can be analyzed using several methods: Langmuir method, BET (Brunauer–Emmett–Teller) method, t-plot method, BJH method or NLDFT method [21]. Here, the BET method was used for the adsorption isotherm analysis, and the specific surface areas are 265 $m^2\ g^{-1}$ for GNP3 and GNP5 and 550 $m^2\ g^{-1}$ for GNP8. The measured specific surface areas were found to be smaller than those reported by NNc.

Solutions preparation

Different masses of GNP were dispersed in 20 mL of each base fluid, to obtain the following solid fractions: $\phi = 0.05$, 0.25, 0.45, 0.75 and 1%. For each base fluid, seven GNP solutions were prepared, including five samples with different volume fractions using GNP8 (shown in Fig. 3) and two samples with volume fraction 1% using GNP3 and GNP5, respectively. Here, no dispersing agent nor surfactant has been used. To insure a good mixing and an uniform dispersion of the particles in the base liquid, each mixture was stirred with a magnetic stirrer for 48 h. In order to limit the initial agglomeration of the nanoplatelets due to van der Waal forces and high surface areas, the suspensions were subjected to ultrasonication (BPAC ultrasonic bath, oscillation frequency 40 kHz and power 240 W) for 2 h. The samples, contained in closed vials, were immersed in a water bath at room temperature. Next, all suspensions were stored at room temperature in hermetic containers. No observable phase separation or agglomeration has been detected in the containers before rheological measurements. Moreover, at the beginning of tests, the samples were again stirred and sonicated for 30 min before the measurements.

Methods

The viscosity measurements were performed using a Anton Paar rheometer MCR502 equipped with a convection oven. The temperature was directly measured at the sample height from temperature probe gas-outlet (CTD Pt100) placed inside the oven. The liquid suspension was placed in between concentric stainless-steel cylinders (see schematic in the inset of Fig. 4), with inner diameter 9.99 mm, outer

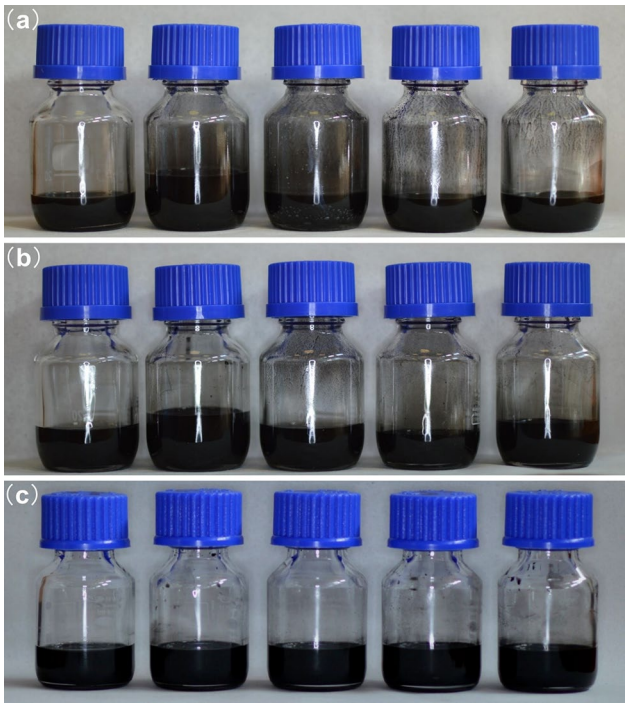

Fig. 3 Pictures of the prepared GNP8 suspensions with GNP concentrations 0.05, 0.25, 0.45, 0.75 and 1% (from left to right). Base fluids are **a** LO, **b** EG and **c** GL

diameter 11 mm and height 29.99 mm. At the bottom of the inner cylinder (bob), there is a cone with a height of 5 mm, and the tip of the cone is placed at about 1 mm from the bottom of the cup.

A constant volume of 5 mL is placed in the cup at room temperature so that the fluid level is slightly higher than the top of the inner cylinder. Then, the oven is closed, and the temperature is set with a soak time from 30 to 60 min with resolution of 0.01 °C. The reported mean steady viscosity and temperature are obtained from the last 10 s interval before the next shear or temperature condition. Each measurement was repeated, and the dispersion is indicated by error bars and is always below 5%.

Results and discussion

Viscosity versus temperature of the base fluids

The rheological tests of the base fluids were carried out first. The data obtained from the experiments for the base fluids are plotted as a function of the temperature, as shown in Fig. 4. Besides, the results for GL, EG and LO were compared to the literature, specifically the results of Takamura et al. [26], Bakak et al. [3] and Segur et al. [24], respectively. It can be seen that the viscosity for each of the base fluids decreases with temperature increasing and that our results are in good agreement with the reference data. An alternative plot is presented in Fig. 4b as a function of $1/T$, where now the increase in viscosity is linear.

Previous authors [20] used an Arrhenius-type law (1) to fit their measurement results of viscosity as a function of temperature. In the present case, the viscosity is also fitted by the Arrhenius law of the form:

$$\eta = A \exp\left(\frac{E_a}{\mathcal{R}T}\right) \tag{1}$$

where the temperature T is in Kelvin, $\mathcal{R} = 8.314\,\mathrm{J\,K^{-1}\,mol^{-1}}$ is the universal gas constant, and E_a is the energy of activation. Using the Arrhenius equation, our experimental measurements led in the case of the three base fluids, to the values of coefficients A and E_a gathered in Table 2 together with the determination coefficients R^2. A coefficient close to 1 indicates a good fit of the model. Large values of E_a indicate that the viscosity is sensitive to temperature. As expected, GL is more thermo-dependent than LO.

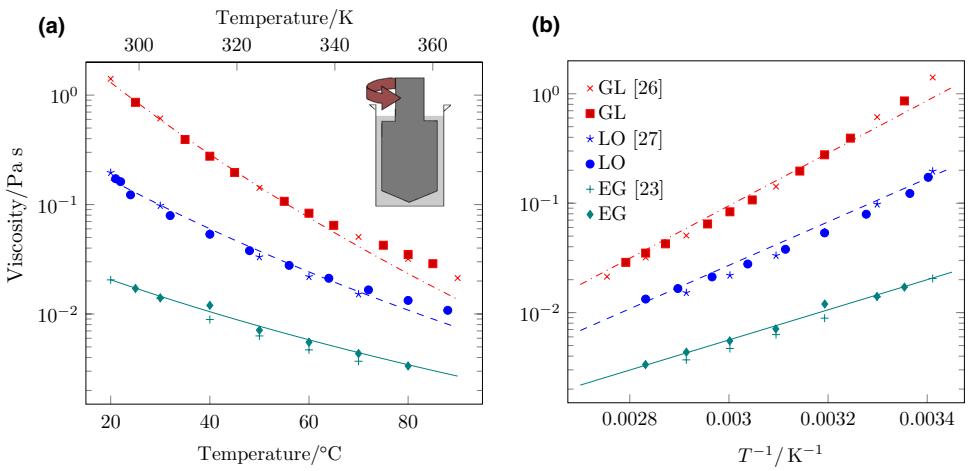

Fig. 4 Shear viscosity of EG, LO and GL as a function of **a** the temperature, T, and **b** $1/T$. The lines represent Arrhenius fits: $\eta(T) = A\exp(E_a/\mathcal{R}T)$ presented in Table 2. The insert is a schematic of the concentric cylinder geometry

Table 2 Parameters of the Arrhenius fit (1) and the coefficient of determination R^2 values used in Fig. 4 for LO, EG and GL base fluids

Fluid	A/Pa s	E_a/kJ mol^{-1}	R^2
LO	1.651×10^{-8}	39.33	0.999
EG	5.545×10^{-7}	25.64	0.982
GL	6.801×10^{-11}	57.71	0.999

Viscosity versus temperature of the suspensions

This investigation is primarily focused on viscosity as it is an important parameters when calculating the heat transfer in flowing fluids. When solid particles are added to base fluids, the study of suspension dynamics shows that the viscosity generally increases in the range $\phi \leq 1\,\%$ of the solid volume fraction [8].

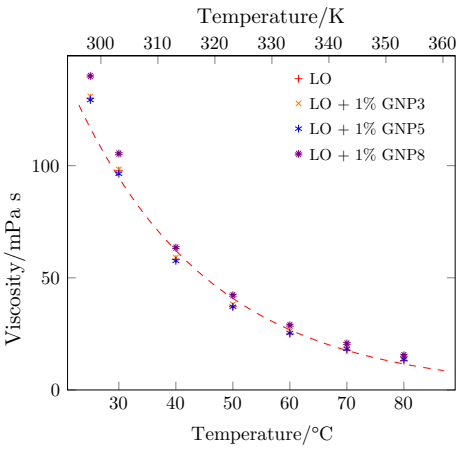

Fig. 6 Viscosity of LO+GNP as a function of T for $\phi = 1\%$ but different SSA at $\dot{\gamma} = 100\ \text{s}^{-1}$. Dashed line represents model (1) for LO

Viscosity

For each base fluid, the temperature protocol described above is reproduced for different concentrations. First, the viscosity at high shear rate is considered, i.e., $\dot{\gamma} = 100\ \text{s}^{-1}$ where the fluid is sheared vigorously but well below the threshold velocity for hydrodynamic inertial instability. Figures 5, 7 and 9 show the viscosity of GNP8 suspension in LO, EG and GL-based fluids for different concentrations, as a function of temperature. The associated Figs. 6, 8 and 10 also show the viscosity at constant solid fraction of 1% as a function of temperature, but for three different specific surfaces areas (SSA): GNP3, GNP5 and GNP8.

In Fig. 5, it can be clearly seen that the viscosity of LO+GNP decreases with the temperature increasing. One can note that the viscosity for low fraction 0.05% is lower than other samples and pure LO at any temperature from 25 to 80 °C, which shows that there is a lubricating phenomenon appearing in LO+GNP with volume fraction $\phi = 0.05\%$. At 25 °C, the viscosity of LO+GNP8 at $\phi = 0.05\%$ is decreased to 120 mPa.s compared to 130 mPa.s for pure LO, which corresponds to a relative decrease of about 8%. It can also be seen from Fig. 6 that the viscosity of LO+GNP is affected slightly by SSA. Only GNP8 with the SSA 550 m^3 g^{-1} experiences an increase in the viscosity.

In Fig. 7, it can be observed that the viscosity of EG+GNP8 nanofluids also decreases at higher temperatures and similar trends have also been observed before [3, 5]. There is an evident increase in viscosity at high concentrations, e.g., at $\phi = 0.75$ and 1%. At the lower temperature below 30 °C, the viscosity of EG+GNP is higher than that of pure EG.

It can be seen in Fig. 8 that the viscosity of EG+GNP with $\phi = 1\%$ and different SSAs is higher than that of pure EG. More specifically, at temperatures below 50 °C, it seems that the SSA has only a small influence on the viscosity increase, but at high temperature, the highest SSA suspension results in the lowest viscosity increase compared to pure EG.

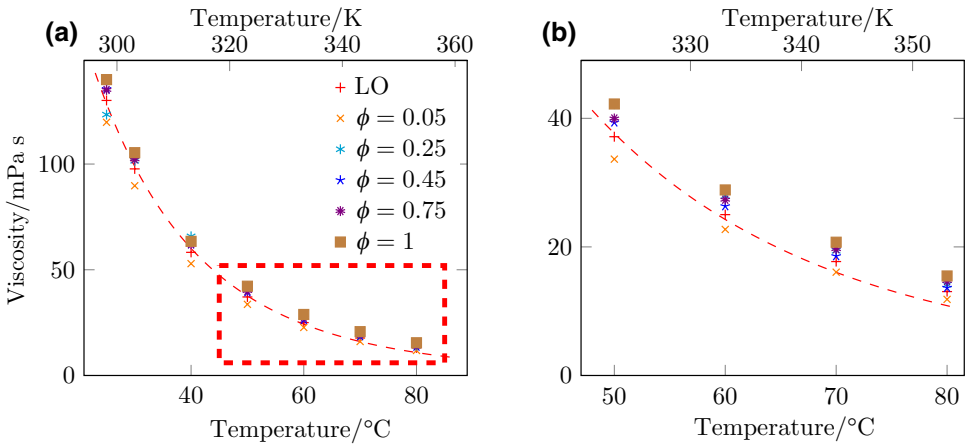

Fig. 5 a Viscosity at $\dot{\gamma} = 100\ \text{s}^{-1}$ of LO and LO+GNP8 as a function of temperature for different fractions, ϕ. (b) Zoom around 50 to 80 °C. Dashed lines represent the model (1) for LO

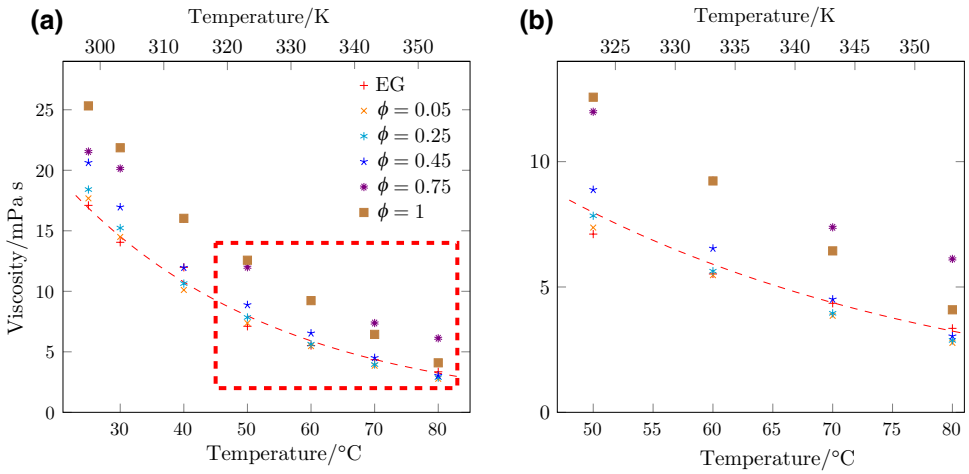

Fig. 7 **a** Viscosity of EG+GNP8 as a function of temperature for different GNP8 fractions, ϕ, at $\dot{\gamma} = 100\ s^{-1}$. **b** Zoom around 50–80°C. Dashed lines represent model (1) for EG

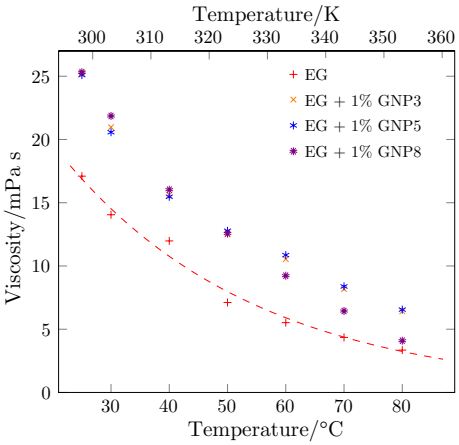

Fig. 8 Viscosity of EG+GNP at $\dot{\gamma} = 100\ s^{-1}$ as a function of temperature for $\phi = 1\%$ and different SSA. Dashed line represents model (1) for EG

From Fig. 9, the viscosity of GL+GNP8 shows the same evolution with increasing temperature as the other suspensions. As in the case of LO+GNP8, we can also observe here a lubricating effect for the GL+GNP8 suspension at 0.05% volume fraction. Finally, it was found here that the viscosity of GL+GNP suspensions increased consistently with increasing SSA, especially at low temperatures, as shown in Fig. 10.

In conclusion, it has been observed here that the viscosity of the different GNP-based suspensions decreases as expected with the temperature, in similar trends than found in previous studies [3, 16]. The significant viscosity increase observed for high GNP concentrations could be explained by particles agglomeration within the suspensions, resulting in internal shear stress and greater force needed for dissipating the agglomeration, hence an increase in viscosity.

Activation energy

After fitting all the viscosity-temperature evolution curves using the Arrhenius law (1), the activation energy E_a and

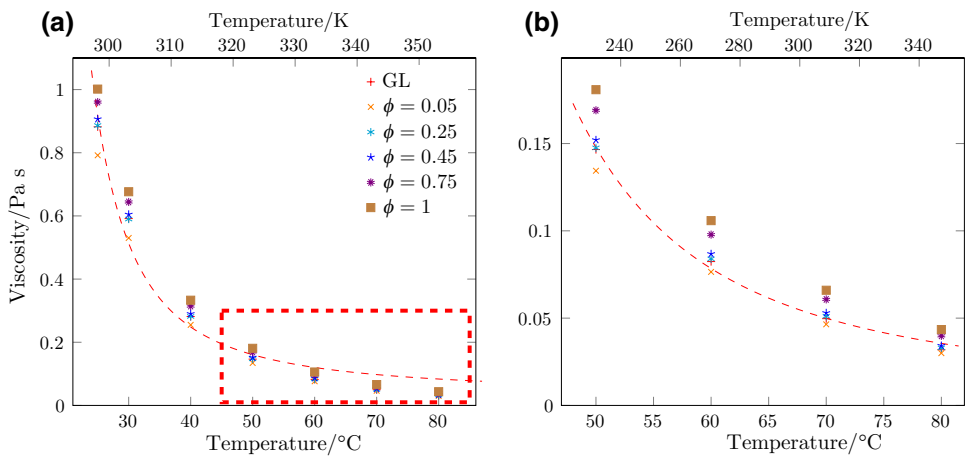

Fig. 9 **a** Viscosity at $\dot{\gamma} = 100\ s^{-1}$ of GL+GNP8 as a function of temperature for different ϕ. **b** Zoom around 50–80 °C. Dashed lines represent model (1) for GL

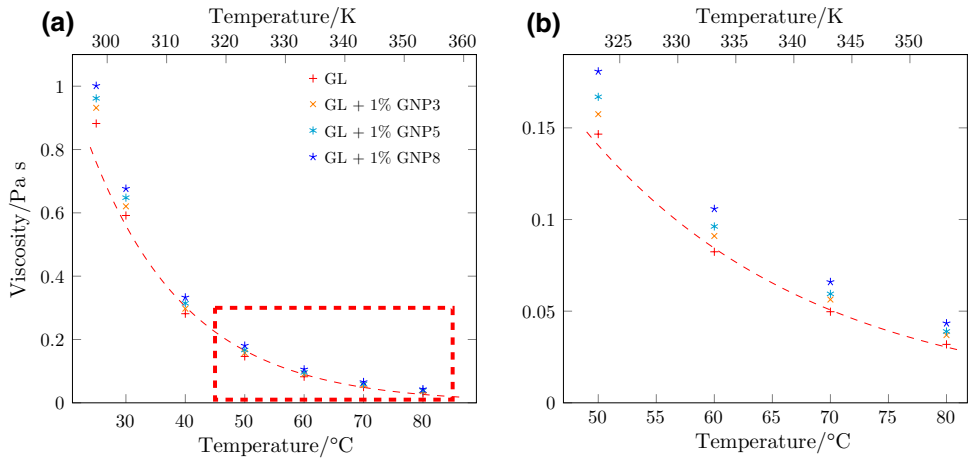

Fig. 10 **a** Viscosity at $\dot{\gamma} = 100$ s^{-1} of GL+GNP $\phi = 1\%$ suspension as a function of temperature but different SSA. **b** Zoom around 50–80 °C. Dashed lines represent model (1) for GL

Table 3 The activation energy E_a (in kJ mol^{-1}) for LO, EG and GL-based suspensions, used in Fig. 11, and the corresponding coefficient of determination R^2 values

ϕ (%)	0.05		0.25		0.45		0.75		0.1		
	E_a	R^2	E_a	R^2	E_a	R^2	E_a	R^2	E_a	R^2	s
LO	39.80	0.999	34.46	0.999	38.85	0.999	38.01	0.999	37.75	0.998	− 0.94
EG	28.44	0.999	28.41	0.999	28.13	0.998	20.10	0.991	25.15	0.993	− 4.49
GL	57.11	0.999	57.75	0.999	57.45	0.999	55.99	0.999	55.09	0.999	− 2.41

The last column indicates the slopes s (in kJ mol^{-1}/%) of the fits

corresponding determination coefficients R^2 have been calculated for each of the suspensions (see Table 3). From the values found for the coefficients of determination, we can see that all the experimental data are well fitted here with Arrhenius' law.

On the whole, the activation energy E_a shows a slight linear downward trend with increasing concentration, as shown in Fig. 11. The decrease is contrast to recent results on graphite polydisperse suspensions in mineral oil [13] that indicates a clear increase in E_a at larger concentration up to 0.25%.

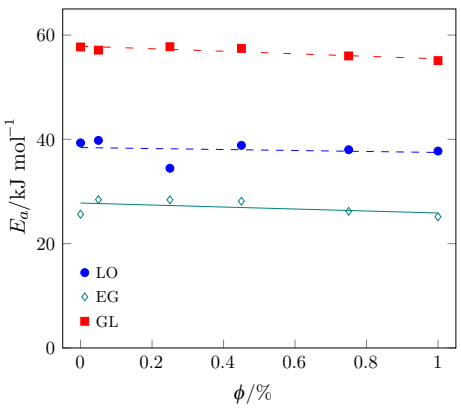

Fig. 11 Evolution of activation energy, E_a, as a function of the GNP8, ϕ, for LO, EG and GL

Effect of the shear rate on viscosity

Figure 12 shows the viscosity behavior at 25 °C of the GNP suspensions as a function of shear rate for different volume fractions, ϕ. Within the shear rates range investigated, $1 \leq \dot{\gamma} \leq 1000$, it is observed that the shear viscosity is dependent on the shear rate and the solid fraction. In comparison with previous experiments [3] using a cone-plate geometry, the present viscosity increase at low shear rate is smaller. Presumably, the concentric cylinder geometry limits slip at the wall but enhances the sedimentation effect that may be present for LO. Bakak et al. [3] used the Carreau–Yasuda (CY) model to fit their rheological measurements results:

$$\frac{\eta - \eta_\infty}{\eta_0 - \eta_\infty} = \left[1 + (\lambda\dot{\gamma})^a\right]^{\frac{n-1}{a}} \tag{2}$$

where η_0 is he zero-shear rate dynamic viscosity, η_∞ is the infinite shear rate dynamic viscosity, and λ is a relaxation time characteristic of the studied fluid; a is a parameter characteristic of the transition width between the zero-shear rate viscosity domain and the shear-thinning domain, and n is the power law index. Unfortunately, the present measurement do not give direct access to η_0 as the zero-shear rate plateau is not clearly observed. Yet, we used the CY model to fit our

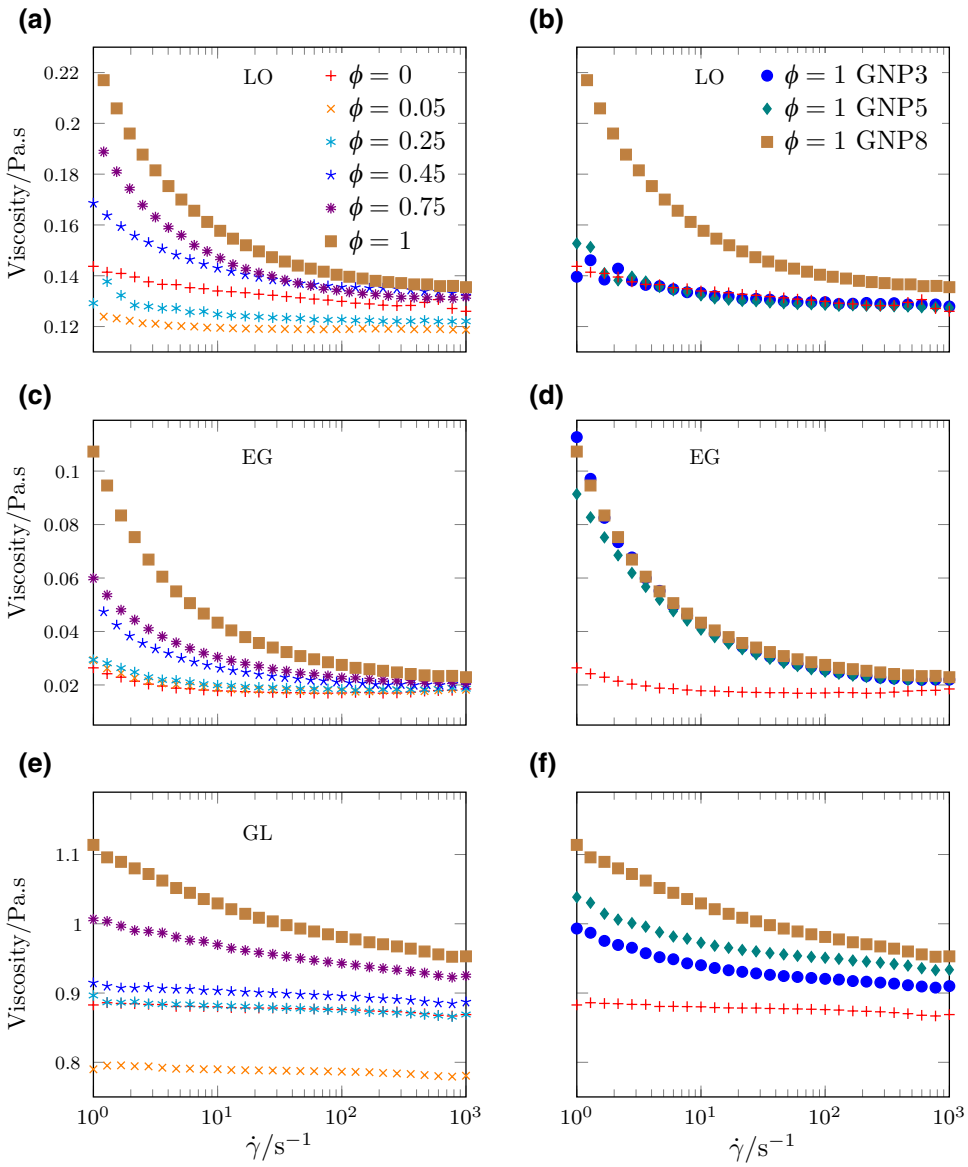

Fig. 12 Viscosity of LO+GNP, EG+GNP and GL+GNP solutions as a function of shear rate $\dot{\gamma}$, **a**, **c**, **e** for different ϕ of GNP8 and **b**, **d**, **f** for different SSA at $\phi = 1\%$ and 25 °C (298.15 K)

data. The fitted values of the CY model parameters, obtained by fitting our experimental results, are presented in Table 4.

When looking at Fig. 12, it is clear that the addition of GNP indices a shear-thinning effect that is more pronounced as ϕ increases. In the case of LO and GL fluids at low ϕ (0.05%), the viscosity remains fairly constant and sometimes have a value below the pure fluid viscosity (see Fig. 12a, e).

For EG (see Fig. 12c, d), the viscosity is the lower of the three fluids tested. However, when GNP are added, there is a systematic increase in viscosity that seems to be independent of GNP SSA (see Fig. 12d).

From Fig. 12e, the viscosity of GL+GNP with 0.05% volume fraction is only smaller than that of pure GL with shear rate varying from 1 to 1000 s^{-1}, indicating that a lubricating effect exists in 0.05% GL+GNP, which is consistent with the conclusion stated before. It can be seen that the viscosity of GNP with concentration 1% increases with SSA increasing in Fig. 12f.

For each of the three studied GNP suspensions, shear-thinning has been observed, which is more pronounced for higher solid volume fractions. As indicated in the literature [17], the decrease in viscosity as a function of shear rate could be attributed to the agglomeration and breakup effect of the GNP or to the alignment of the nanosheets in the plane of flow during shearing, resulting in less viscous dissipation and in a decreasing of the apparent viscosity.

Effect of solid volume fraction on viscosity

The influence of the GNP volume fractions ($\phi = 0.05$, 0.25, 0.45, 0.75 and 1%) on the dynamic viscosity of each of the three base fluids at the working temperature 25 °C is examined

Table 4 Values of the CY model parameters η_0, η_∞, a, λ and n obtained by fitting the experimental results at 25 °C (298.15 K) in the range of shear rate: $1 < \dot{\gamma} < 1000\ s^{-1}$

GNP	Base fluid	ϕ	η_0/Pa s	η_∞/Pa s	a	λ/s	n	R^2_{CY}
8	LO	0.05	0.1240	0.1189	14.045	0.75	− 0.0785	0.992
8	LO	0.25	0.2610	0.1224	9.6960	8.54	0.0310	0.959
8	LO	0.45	0.2352	0.1325	8.8051	7.23	0.4662	0.999
8	LO	0.75	0.3586	0.1295	9.6256	8.86	0.4281	0.999
8	LO	1	0.3998	0.1337	8.1089	6.24	0.4235	0.999
5	LO	1	0.3084	0.1297	11.490	12.36	0.2090	0.971
3	LO	1	0.1420	0.1284	7.7975	0.54	0.3433	0.933
8	EG	0.05	0.1765	0.0178	31.302	17.17	0.0267	0.996
8	EG	0.25	0.1431	0.0183	14.842	19.08	0.1882	0.998
8	EG	0.45	0.1384	0.0196	10.859	7.89	0.3410	0.998
8	EG	0.75	0.1689	0.0204	14.377	9.56	0.4033	0.999
8	EG	1	0.2879	0.0220	8.6131	6.70	0.3972	0.999
5	EG	1	0.2872	0.1091	8.4385	11.41	0.4679	0.999
3	EG	1	0.3310	0.0209	13.681	7.11	0.3654	0.998
8	GL	0.05	0.8332	0.7867	125.13	3.15	− 0.4967	0.919
8	GL	0.25	0.8967	0.7563	8.1862	6.27	0.9734	0.943
8	GL	0.45	1.0669	0.8989	74.525	9.21	− 0.9766	0.945
8	GL	0.75	1.0858	0.8787	0.8620	20.47	0.8450	0.998
8	GL	1	1.2817	0.9151	1.0755	12.31	0.7573	0.999
5	GL	1	1.1886	0.9297	7.5546	10.18	0.6175	0.994
3	GL	1	1.0780	0.9042	7.4179	5.56	0.6091	0.997

in the following in Fig. 13, for different shear rates, $\dot{\gamma} = 1$, 10, 100 and 10,000 s^{-1}. For each fluid LO, EG and GL, the relative viscosity defined as the ratio of the shear viscosity to the shear viscosity without GNP is represented as a function of the GNP volume fraction. In order to take into account ϕ, the relative viscosities are modeled using the law proposed by Vallejo et al. [28]:

$$\eta = \eta_0 \exp\left(\frac{DT_0}{T - T_0}\right) + E\phi \exp\left(\frac{F}{T}\right) - G\phi^2 \tag{3}$$

where the parameters η_0, D and T_0 values are obtained from modeling the data of the base fluids using Vogel–Fulcher–Tammann (VFT) equation [28]:

$$\eta = \eta_0 \exp\left(\frac{DT_0}{T - T_0}\right) \tag{4}$$

E, F, and G are fitting parameters, and ϕ is the volume fraction. Considering only a constant temperature $T_0 = 25$ °C, Vallejo's law can be expressed in the following form:

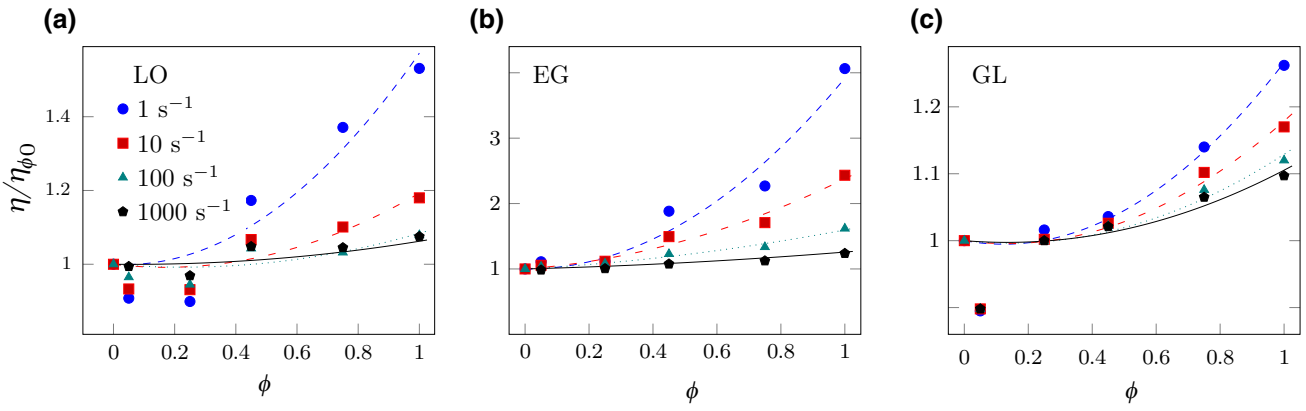

Fig. 13 Relative viscosity of **a** LO+GNP8, **b** EG+GNP8 and **c** GL+GNP8 as a function of the solid fraction at temperature 25 °C for different shear rates: $1 \leq \dot{\gamma} \leq 1000\ s^{-1}$. The dashed lines correspond to the model (3) described in the text

$$\frac{\eta}{\eta_{\phi_0}} = 1 + \frac{F}{\eta_{\phi_0}}\phi - \frac{G}{\eta_{\phi_0}}\phi^2 \quad (5)$$

where η_{ϕ_0} is the viscosity of the base fluids at temperature T, F and G are fitting parameters.

After fitting the data of viscosity with volume fraction using the model (5) for different shear rates in the case of EG, the model describes well the suspension viscosity as a function of GNP volume fraction ϕ as found in the study of Bakak et al. [3]. For GL and EG, the fits did not take into account the lubricating points. Hence, the results of fitting the Vallejo model are in good agreement with the data. For EG, the increase in viscosity is more important as the shear rates considered are low. For example, for $\dot{\gamma} = 1\ s^{-1}$ and $\phi = 1\%$, it is found that the relative increase in viscosity is $\eta/\eta_{\phi_0} \approx 4.06$.

Moreover, the evolution of the relative viscosity of the GNP with ϕ leads to several observations. There is a weak lubricating effect in LO+GNP, at the limit of the measurement uncertainty, for the volume fraction considered ($\phi = 0.05$ and 0.25%). The relative viscosity of LO+GNP for volume fractions 0.05 and 0.25% is smaller than one. For shear rates investigated, the lubricating effect at low shear rate is more evident than that at high shear rate. It can be seen that for the GL+GNP, there is also a noticeable lubricating effect for the volume fraction $\phi = 0.05\%$; the viscosity reduces about 10% at the shear rates investigated compared to pure GL. The possibility of a lubrication effect, in the case of the LO+GNP and GL+GNP for solid volume fractions, which should allow a significant improvement in heat extraction, is a very encouraging result for the use of these liquids from an industrial point of view. For higher volume fractions given by 0.75 and 1%, the viscosity becomes greater than that of the base fluids, whatever the shear rate considered. For EG suspension, there is no lubricating effect appearing. Since the GNP is of the same nature for the three types of suspension considered in this study, this difference in behavior should be attributed to the base fluid-GNP interactions.

Conclusions

An experimental study of the rheological properties of GNP suspension was presented for the following base fluids: LO, EG and GL. The GNP suspension was prepared by ultrasonication and stirring that were stable for a relatively long period of time. Detailed shear viscosity measurements were carried out to determine the effect of particles volume concentration, specific surface area, shear rate and temperature on the shear viscosity properties of GNP suspension. The results indicate that temperature has a strong effect on the viscosity properties, which decreases significantly with increasing temperature.

It can be noted that shear-thinning exists, and there is a plateau at high shear rate range in the viscosity versus shear rate plots. The decrease in viscosity as a function of shear rate could be attributed to the breakup of agglomeration of graphene nanosheets or to the alignment of the nanosheets in the plane of flow during shearing. The shear viscosity properties can be reproduced using the CY model, which gives good approximation for the three base fluids considered. The influence of GNP concentration on the shear viscosity properties has been systematically studied, for different solid volume fractions (0.05, 0.25, 0.45, 0.75 and 1%). Shear tests on suspension revealed that higher concentration increases the viscosity; however, other investigated parameters, such as specific surface area, have a small influence on the viscosity too.

The low concentration (0.05%) GNP in LO and GL experience a lubrication effect in which the viscosity decreases with the addition of graphene nanoparticles. This interesting behavior allows to consider industrial applications for this suspensions in the field of heat extraction, for example.

Future works will focus on the thermal and thermodynamic properties, such as thermal conductivity and specific heat, and on the electrical and dielectric properties.

Acknowledgements The authors thank Prof. Philippe Barboux for the BET measurements.

Author contributions JB, RH, GR, AA and JP contributed to the conception and design of the study. JB and JP acquired the data. JB, RH and JP analyzed or interpreted the data. JB and JP drafted the manuscript. RH, GR, AA and JP revised the manuscript. All authors have read and agreed to the published version of the manuscript

Funding The authors declare that no funds, grants or other support were received during the preparation of this manuscript.

Declarations

Conflict of interest On behalf of all authors, the corresponding author states that there is no conflict of interest. The authors have no relevant financial or non-financial interests to disclose.

References

1. Ahammed N, Asirvatham LG, Wongwises S. Effect of volume concentration and temperature on viscosity and surface tension of graphene-water nanofluid for heat transfer applications. J Therm Anal Calorim. 2016;123(2):1399–409. https://doi.org/10.1007/s10973-015-5034-x.
2. Arshad A, Jabbal M, Yan Y, et al. A review on graphene based nanofluids: preparation, characterization and applications. J Mol Liq. 2019;279:444–84. https://doi.org/10.1016/j.molliq.2019.01.153.

3. Bakak A, Lotfi M, Heyd R, et al. Viscosity and rheological properties of graphene nanopowders nanofluids. Entropy. 2021;23(8):979. https://doi.org/10.3390/e23080979.
4. Bortolato M, Dugaria S, Agresti F, et al. Investigation of a single wall carbon nanohorn-based nanofluid in a full-scale direct absorption parabolic trough solar collector. Energy Convers Manag. 2017;150:693–703. https://doi.org/10.1016/j.enconman.2017.08.044.
5. Cabaleiro D, Colla L, Barison S, et al. Heat transfer capability of (ethylene glycol+water)-based nanofluids containing graphene nanoplatelets: design and thermophysical profile. Nanoscale Res Lett. 2017;12(1):1–11. https://doi.org/10.1186/s11671-016-1806-x.
6. Cong P, Xu P, Chen S. Effects of carbon black on the anti-aging, rheological and conductive properties of sbs/asphalt/carbon black composites. Constr Build Mater. 2014;52:306–13. https://doi.org/10.1016/j.conbuildmat.2013.11.061.
7. Fakhari A, Fernandes C, Galindo-Rosales FJ. Mapping the volume transfer of graphene-based inks with the gravure printing process: influence of rheology and printing parameters. Materials. 2022;15(7):2580. https://doi.org/10.3390/ma15072580.
8. Guazzelli E, Morris JF. A physical introduction to suspension dynamics. Cambridge: Cambridge University Press; 2011. https://doi.org/10.1017/CBO9780511894671.001.
9. Halelfadl S, Estellé P, Aladag B, et al. Viscosity of carbon nanotubes water-based nanofluids: influence of concentration and temperature. Int J Therm Sci. 2013;71:111–7. https://doi.org/10.1016/j.ijthermalsci.2013.04.013.
10. Hamze S, Cabaleiro D, Estellé P. Graphene-based nanofluids: a comprehensive review about rheological behavior and dynamic viscosity. J Mol Liq. 2021;325(115):207. https://doi.org/10.1016/j.molliq.2020.115207.
11. Iranmanesh S, Mehrali M, Sadeghinezhad E, et al. Evaluation of viscosity and thermal conductivity of graphene nanoplatelets nanofluids through a combined experimental-statistical approach using respond surface methodology method. Int Commun Heat Mass Transf. 2016;79:74–80. https://doi.org/10.1016/j.icheatmasstransfer.2016.10.004.
12. Kole M, Dey TK. Investigation of thermal conductivity, viscosity, and electrical conductivity of graphene based nanofluids. J Appl Phys. 2013;113(8): 084307. https://doi.org/10.1063/1.4793581.
13. Larsen T, Søbye AL, Royer JR, et al. Rheology of polydisperse nonspherical graphite particles suspended in mineral oil. J Rheol. 2022;67(1):81–9. https://doi.org/10.1122/8.0000511.
14. Lee GJ, Rhee CK. Enhanced thermal conductivity of nanofluids containing graphene nanoplatelets prepared by ultrasound irradiation. J Mater Sci. 2014;49(4):1506–11. https://doi.org/10.1007/s10853-013-7831-6.
15. Lotfi M, Heyd R, Bakak A, et al. Experimental measurements on the thermal conductivity of glycerol-based nanofluids with different thermal contrasts. J Nanomater. 2021. https://doi.org/10.1155/2021/3190877.
16. Mehrali M, Sadeghinezhad E, Latibari ST, et al. Investigation of thermal conductivity and rheological properties of nanofluids containing graphene nanoplatelets. Nanoscale Res Lett. 2014;9(1):1–12. https://doi.org/10.1186/1556-276X-9-15.
17. Moghaddam MB, Goharshadi EK, Entezari MH, et al. Preparation, characterization, and rheological properties of graphene-glycerol nanofluids. Chem Eng J. 2013;231:365–72. https://doi.org/10.1016/j.cej.2013.07.006.
18. Novoselov KS, Geim AK, Morozov SV, et al. Electric field effect in atomically thin carbon films. Science. 2004;306(5696):666–9. https://doi.org/10.1126/science.1102896.
19. Pavía M, Alajami K, Estellé P, et al. A critical review on thermal conductivity enhancement of graphene-based nanofluids. Adv Coll Interface Sci. 2021;294(102):452. https://doi.org/10.1016/j.cis.2021.102452.
20. Peixinho J, Karanjkar PU, Lee JW, et al. Rheology of hydrate forming emulsions. Langmuir. 2010;26(14):11699–704. https://doi.org/10.1021/la101141j.
21. Ruthven DM. Principles of adsorption and adsorption processes. Hoboken: Wiley; 1984.
22. Sadeghinezhad E, Mehrali M, Saidur R, et al. A comprehensive review on graphene nanofluids: recent research, development and applications. Energy Convers Manag. 2016;111:466–87. https://doi.org/10.1016/j.enconman.2016.01.004.
23. Sandeep N. Effect of aligned magnetic field on liquid thin film flow of magnetic-nanofluids embedded with graphene nanoparticles. Adv Powder Technol. 2017;28(3):865–75. https://doi.org/10.1016/j.apt.2016.12.012.
24. Segur JB, Oberstar HE. Viscosity of glycerol and its aqueous solutions. Ind Eng Chem. 1951;43(9):2117–20. https://doi.org/10.1021/ie50501a040.
25. Soares YCF, Cargnin E, Naccache MF, et al. Influence of oxidation degree of graphene oxide on the shear rheology of poly (ethylene glycol) suspensions. Fluids. 2020;5(2):41. https://doi.org/10.3390/fluids5020041.
26. Takamura K, Fischer H, Morrow NR. Physical properties of aqueous glycerol solutions. J Petrol Sci Eng. 2012;98:50–60. https://doi.org/10.1016/j.petrol.2012.09.003.
27. Vakili M, Khosrojerdi S, Aghajannezhad P, et al. A hybrid artificial neural network-genetic algorithm modeling approach for viscosity estimation of graphene nanoplatelets nanofluid using experimental data. Int Commun Heat Mass Transf. 2017;82:40–8. https://doi.org/10.1016/j.icheatmasstransfer.2017.02.003.
28. Vallejo JP, Żyła G, Fernández-Seara J, et al. Influence of six carbon-based nanomaterials on the rheological properties of nanofluids. Nanomaterials. 2019;9(2):146. https://doi.org/10.3390/nano9020146.
29. Wang Y, Al-Saaidi HAI, Kong M, et al. Thermophysical performance of graphene based aqueous nanofluids. Int J Heat Mass Transf. 2018;119:408–17. https://doi.org/10.1016/j.ijheatmasstransfer.2017.11.019.